Review

Abrasive Resistant Coatings—A Review

Linmin Wu, Xingye Guo and Jing Zhang *

Department of Mechanical Engineering, Indiana University—Purdue University Indianapolis, Indianapolis, IN 46202, USA; E-Mails: lw54@umail.iu.edu (L.W.); xingguo@umail.iu.edu (X.G.)

* Author to whom correspondence should be addressed; E-Mail: jz29@iupui.edu;
   Tel.: +1-317-278-7186.

Abstract: Abrasive resistant coatings have been widely used to reduce or eliminate wear, extending the lifetime of products. Abrasive resistant coatings can also be used in certain environments unsuitable for lubrications. Moreover, abrasive resistant coatings have been employed to strengthen mechanical properties, such as hardness and toughness. Given recently rapid development in abrasive resistant coatings, this paper provides a review of major types of abrasive coatings, their wearing mechanisms, preparation methods, and properties.

Keywords: coating; abrasive resistant; wear; tribology; roughness; mechanical properties

1. Introduction

In most working conditions, wear is minimized by applying lubrication to improve surface mechanical properties. However, in some situations, oil or grease lubrications alone are not sufficient to meet wear resistance requirements. Abrasive resistant coatings may be the only feasible option to protect the product surfaces. In situation where operating temperatures are extremely high, operating time is long, or the environments (e.g., vacuum, radioactivity, *etc.*) are not suitable for lubricants [1], abrasive resistant coatings provide a better option. In such situations, abrasive resistant coating is an attractive means to resolve the surface wear issues.

Wear occurs during abrasion between two contact surfaces due to uneven or rough profiles. When bumpy surfaces contact each other, abrasive forces occur. If a material does not meet wear requirement even with lubrication, coatings with improved anti-abrasive properties may be required.

Given recently rapid development in abrasive resistant coatings, the following discussion provides a review of major coating types, their wearing mechanisms, preparation methods, and relevant properties.

2. Abrasive Wear Mechanisms

Abrasive wear occurs when a hard rough surface slides over another surface [2–5]. The American Society for Testing and Materials (ASTM) International defines it as the loss of material due to hard particles that are forced against and move along a solid surface [6].

Abrasive wear is commonly classified based on the type of contact and contact environments [7]. The type of contact determines the mode of abrasive wear. Two modes of abrasive wear are known as two-body and three-body abrasive wear. Two-body wear occurs when the grits or hard particles remove material from the opposite surface. The common analogy is that material being removed or displaced by a cutting or plowing operation. Three-body wear occurs when the particles are not constrained, and are free to roll and slide down a surface [3,8].

There are a number of factors which influence the abrasive wear and, hence, the manner of material removal. Several different mechanisms have been proposed to describe the manner in which the material is removed. Three commonly identified mechanisms of abrasive wear are: plowing, cutting, and fragmentation. Plowing occurs when material is displaced to the side, away from the wear particles, resulting in the formation of grooves that do not involve direct material removal. The displaced material forms ridges adjacent to grooves, which may be removed by subsequent passage of abrasive particles. Cutting occurs when material is separated from the surface in the form of primary debris, or microchips, with little or no material displaced to the sides of the grooves. This mechanism closely resembles conventional machining. Fragmentation occurs when material is separated from a surface by a cutting process and the indenting abrasive causes localized fracture of the wear material. These cracks then freely propagate locally around the wear groove, resulting in additional material removal by spalling [7].

Williams and Hyncica correlated abrasive wear with the movement of abrasive particles at the interface in lubricated contacts [9]. These authors proposed that the particle movement defines the material removal mechanism. This particle movement in turn depends on the particle size and shape and the distance between the sliding surfaces, thus promoting wear transitions from rolling to plowing to cutting [9].

During abrasive wear, different wear mechanisms can lead to material removal. The sliding of fixed particles causes scratches on the antagonist surface. A sequence of scratches may be used to simulate the sliding of the particles. Each scratch induces microcutting and/or microplowing and/or microcracking [10]. The rolling of abrasive particles at the interface results in multiple indentations. Moreover, the rolling of abrasive particles can be simulated using a sequence of indentations. Each indentation may induce ductile or brittle behaviors of the material. Rolling and sliding together cause a mixture of indentations and scratches on the surfaces [11].

Buijs and Korpel-van Houten investigated the abrasive wear mechanisms during the lapping of optical glasses [12]. They proposed a model in which the rolling of abrasive particles can lead to material removal when the load per particle achieves the threshold value for lateral cracking. They also showed that the particle dynamics depend on the counter-body hardness, due to the fact that softer counter bodies, particle sliding becomes more significant than rolling.

The abrasion efficiency is described by the parameter f_{ab}, the ratio material removed to the volume of the scratch [13]:

$$f_{ab} = \frac{A_V - (A_1 + A_2)}{A_V} \quad (1)$$

where A_V is the groove area measured relative to the plane of the original surface, while A_1 and A_2 are the cross sectional areas of the plastically deformed ridges on either side of the groove. If the material undergoes brittle fracture, then spalling of the surface can result in A_1 and A_2 having negative values. Ductile materials tend to exhibit cutting efficiencies f_{ab} less than 1, while for brittle materials f_{ab} can be greater than 1.

Values of f_{ab} ranging from 0.15 to 1.0 have been found for 30 different metals and alloys [14]. For these conditions, f_{ab} can be approximated by:

$$f_{ab} = 1 - (\frac{\varphi_{lim}}{\varphi_s})^{\sqrt[3]{\frac{8H}{H_{def}}}} \quad (2)$$

where H_{def} is the hardness of the deformed material or wear debris, H is the undeformed material hardness, φ_s is the effective strain imposed by the scratch, and φ_{lim} is the effective strain required for cutting [13].

Using a thin coating, a wear resistant material of submicrons in thickness, the best properties concerning friction and wear will be located where they are most needed, while the substrate acts as a load carrier. The substrate should be able to resist mechanical fracture failure as well as deformation of tool geometry while the coating should be designed to resist surface deterioration. Further, when depositing a coating, an interface is introduced and its strength, *i.e.*, the adhesion, is of great importance to avoid spalling of the coating. In pure adhesion, the interfacial atomic binding forces are of importance as is the potential of the coating system to decrease the shear stresses in the interface has a large influence. To gather the mechanical and tribological requirements and thus the tool's operational functionality, the coating system (*i.e.*, substrate, interface, and coating) has to obtain an appropriate combination of properties. Hence, the substrate may have a high strength and toughness while the coating must be hard, chemically stable and wear resistant. In addition, thermal expansion, shear strength, as well as elasticity of the components matter. In order to increase the interfacial strength, all the above mentioned properties have to be optimized. These properties are dependent of many factors, such as chemical and phase composition, coating architecture, thickness, texture, microstructure, porosity, defect density, residual stress state, as well as surface topography of the coating. In turn, these coating characteristics are controlled by different deposition process parameters, e.g., temperature, pressure, and gas flow. In addition, the understanding of the relationship between process parameters, coating characteristics, and finally tribological characteristics is needed in order to develop the coating materials [15].

A surface may be scratched, grooved, or dented by a harder particle to produce one or more effects [16]. Scratching implies some loss of materials, whereas grooving does not. Scratches and grooves may be no deeper than the thickness of the coatings. This may occur if the abrasive particles are softer than the substrate but harder than the coating, or it may occur if the abrasive particles are very small. Groove or scratch widths will probably be of the order of coating thickness. Generally, these fine scratches are not

discernible and thus the surface appears polished. The centers of diffraction of the scratches are separated at a distance much less than the wavelength of the light, *i.e.*, <0.1 μm [16].

The scratches, grooves, and dents may penetrate into the substrate. Deep scratching will provide debris of the substrate materials. An abrasive particle is abrasive only if it scratches (grooves or dents), and for that purpose the abrasive material must be harder than the surface [16].

3. Relevant Materials Properties and Processing Considerations

Abrasive wear of materials depends on many factors, including roughness, hardness, toughness, and contact geometry. Processing techniques to modify these factors are summarized below.

3.1. Roughness

Roughness is a measure of the texture of a surface. It is quantified by the vertical deviations of a real surface from its ideal form. If the deviations are large, the surface is rough; if they are small, the surface is smooth. Roughness plays a critical role in determining how the coating interacts with its environment. Rough surfaces usually wear more quickly and have higher friction coefficients than smooth surfaces.

The average roughness R_a is defined as follows [17]:

$$R_a = \frac{1}{n}\sum_1^n |y_i| \qquad (3)$$

where y is the height at the measurement point i; n is the total number of measurement points.

In a study of nitrocarburized DC53 tool steels [18], the untreated specimen and the 2, 4, 6-h nitrocarburized specimens were marked as NC-0, NC-2, NC-4, and NC-6, respectively. The surface roughnesses of the specimens were measured before and after the block-on-roller wear test. After nitrocarburizing, the surface roughness increased due to the formation of nitrides on the surface (Figure 1). After the wear tests, the surface roughness of specimen NC-0 increased because of stronger adhesive tracks, while the roughness of the specimens after nitrocarburizing decreased due to the polishing effect [18].

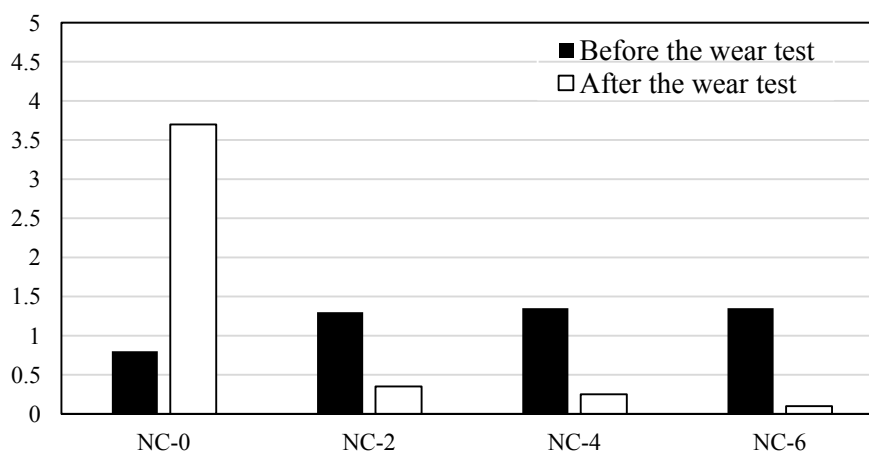**Figure 1.** Surface roughness of the tested specimens before and after the wear tests [18].

Figure 2 shows the cross-sections and surfaces of coatings formed in the alkaline silicate electrolyte containing K_2ZrF_6 without titania sol (coating A), and with titania sol (coating B). Coating A was composed of MgO, Mg_2SiO_4, and ZrO_2, and coating B was composed of MgO, TiO_2, and ZrO_2. There were no fracture sites in the cross-section views of both coatings. Compared with coating A, the surface of coating B was more uniform and smoother, and the number of micropores decreased with the increase of diameter, indicating coating B had better tribological properties [19].

Figure 2. SEM images of cross-sections and surfaces of coating A (**a**,**c**) and coating B (**b**,**d**) formed in the alkaline silicate electrolyte containing K_2ZrF_6 without and with the addition of titania sol, respectively [19].
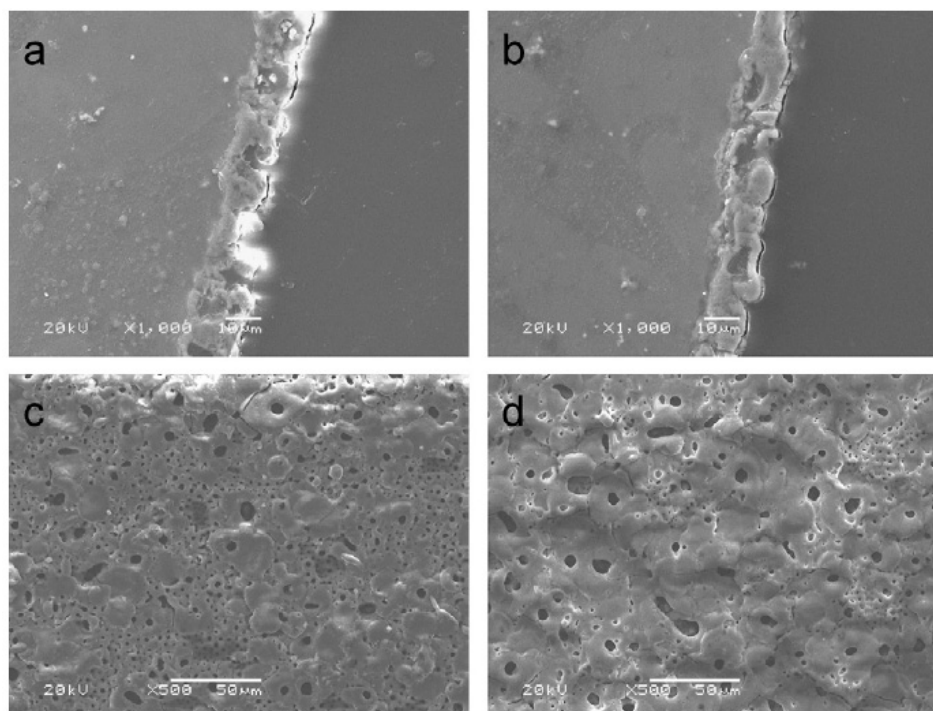

For WC-Co-Al_2O_3 coatings deposited by the electro-spark method, the roughness was in the range from 6.16 to 7.79 μm. After the laser treatment, R_a was changed in the range from 8.12 to 9.03 μm. The steel specimens (C45) without coatings had a roughness from 0.39 to 0.41 μm [20]. This indicated that the laser treatment made the smoother surface.

Mezlini *et al.* investigated the transitions of wear mechanisms in aluminum alloys through studying the interactions in single scratch tests [21]. They produced two parallel scratches with a defined distance between them and then a third parallel scratch in the middle of the previous ones. They found that the wear mechanism changed from plowing and wedge formation for a single scratch to cutting when the scratches interacted with each other [21].

Mo and Zhu applied the multi-arc ion plating technique to obtain CrN and AlCrN coatings. The surface roughness of AlCrN ($R_a = 0.12 \pm 0.01$ μm) was lower than that of CrN ($R_a = 0.21 \pm 0.11$ μm) [22], suggesting the content of Al can make the coatings smoother. Figure 3 shows the wear morphology of the CrN and AlCrN coatings when sliding against Si_3N_4 ceramic under a normal load of 20 N. For the CrN coatings, failure was observed in the middle of the wear scar. The detached coatings crushed into fine particles to form a debris layer. The maximum depth of the deep pit (approximately 1.5 μm) was

smaller than that of the coating (approximately 2.1 μm), indicating a delamination mechanism. No severe wear was found for the AlCrN coatings. AlCrN exhibited a smooth worn surface with a high debris removal efficiency [22].

Figure 3. Wear scar morphology of the coatings when sliding against Si_3N_4 ceramic under a normal load of 20 N: (**a**) CrN and (**b**) AlCrN [22].
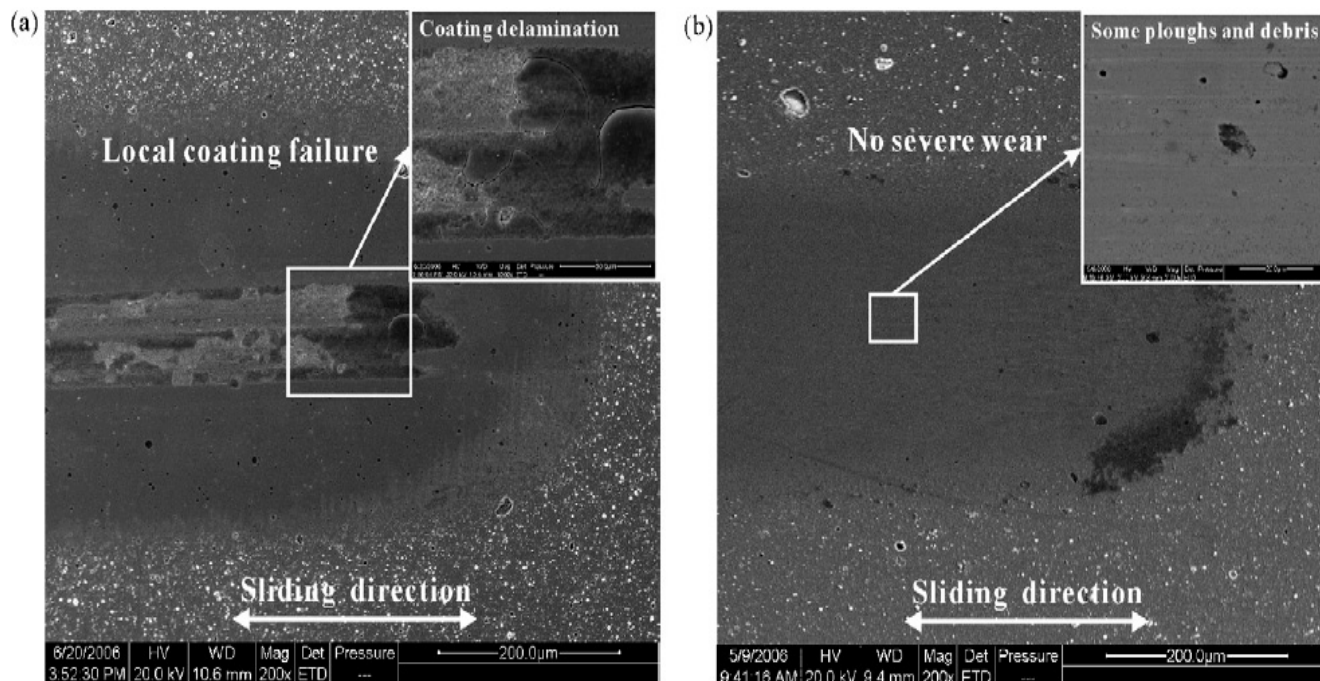
Zhang *et al.* [23] employed a novel silicate based lubricant additive to 300-h pin-on-disk tribological tests. The surface roughness of the specimens before the wear test was 0.8 μm. After the 300-h friction and wear tests, the surface roughness was reduced greatly. The surface roughness became 60.318 nm for the disk, and 8.053 nm for the pin [23]. Figure 4 shows the roughness of wear track on the coatings, with marked maximum wear depths. The wear tracks on TiN and TiAlN were relatively smooth, but AlTiN showed large grooves [24].

Peak voltage and pulse frequency in the deposition have a great effect on the roughness of the formed DLC (diamond-like carbon) films, using asymmetric bipolar pulsed plasma deposition. As shown in Figure 5, the roughness increased with an increase of peak voltage. Surface roughness was under 0.5 nm RMS (root mean square) in general, whereas the highest value approximately 1 nm RMS was achieved at 1400 V. At high RMS values, it was easy for debris to be released from the surface during the wear test, causing abrasive suspension. In Figure 5, it can be seen that the increase of roughness at higher peak voltage was attributed to the enlargement of both grain diameter and peak-to-valley distance [25].

Figure 4. The roughness of wear tracks on the coatings: (**a**) TiN; (**b**) TiAlN; (**c**) AlTiN; and (**d**) CrAlN [24].
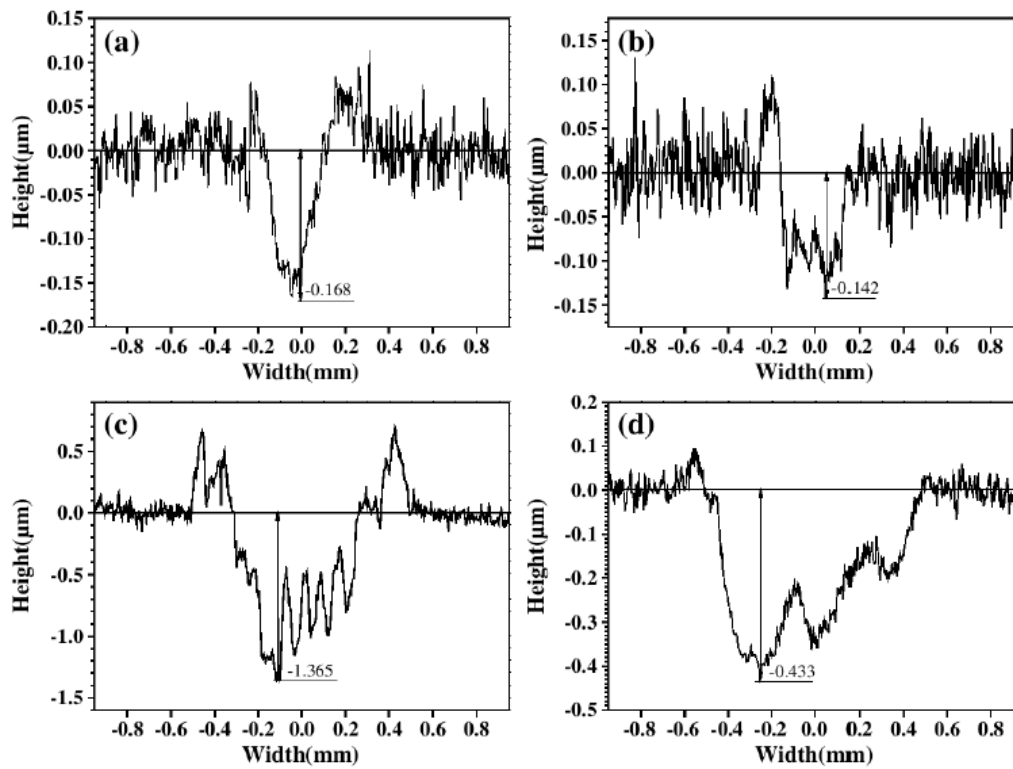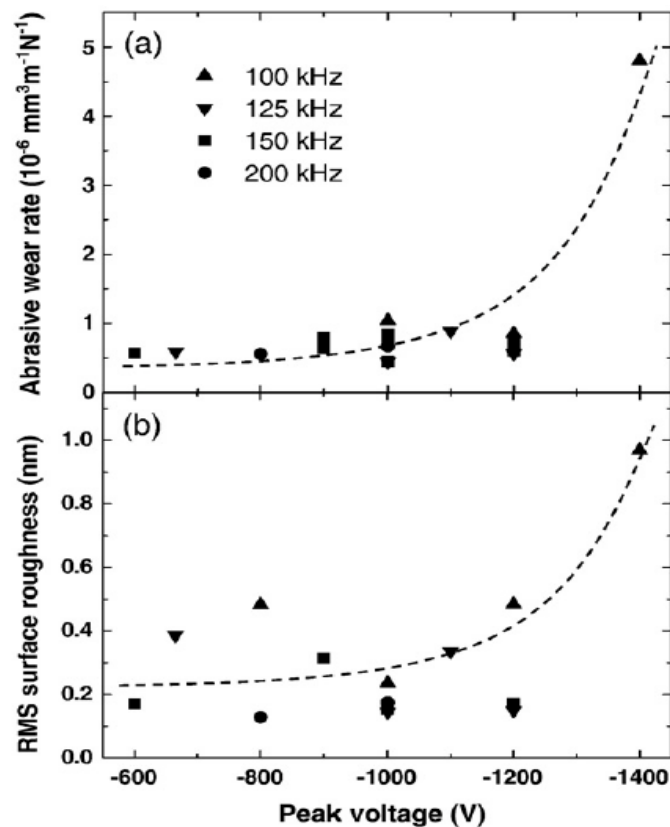

Figure 5. Influence of peak voltage on surface roughness and abrasive wear rate of DLC films deposited at different pulse frequencies [25].

3.2. Hardness and Toughness

Hardness measurements quantify the resistance of a material to plastic deformations. Indentation hardness tests include the majority of processes used to determine the hardness. Hardness, however, cannot be considered to be a fundamental material property. Instead, it represents an arbitrary quantity used to provide a relative idea of material surface properties [26]. The equation based definition of hardness is the pressure applied over the contact area between the indenter and the material being tested. As a result, hardness values are typically reported in units of pressure.

Hardness of coatings can be modified by preparation methods and conditions. The hardness of hydroxyapatite (HA) coatings deposited by using gas tunnel type plasma spraying was influenced by arc currents, as shown in Figure 6. The hardness of the coatings increased with the increasing arc current because of the formation of dense HA coatings [27]. The morphologies of the spayed HA coatings are shown in Figure 7. At low arc current (350 A), the coatings had a lot of pores and unmelted powders. As the arc current increased to 500 A, the sprayed coatings became denser. The dense structure of HA coatings was the consequence of increasing the plasma power which led to the melting HA particles [27].

Figure 6. Hardness and porosity values of HA coatings sprayed at different arc currents [27].
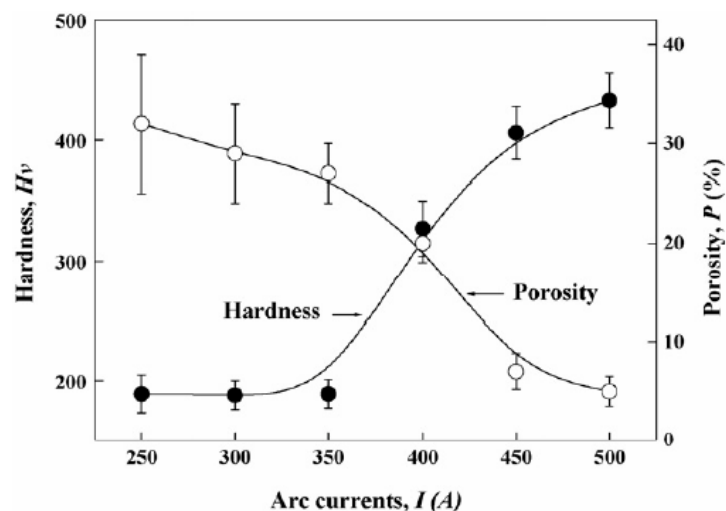
The microstructure in the electrospark alloying WC-Co-Al$_2$O$_3$ coating before and after treatment with an Nd:YAG laser is shown in Figure 8. The laser-modified outer layer did not have microcracks or pores. There was no discontinuity of the coating-substrate boundary. The laser-treated WC-Co-Al$_2$O$_3$ coating was thicker. Furthermore, the heat affected zone (HAZ) was larger, and the carbon content in the zone was higher [20]. The microhardness of WC-Co-Al$_2$O$_3$ coatings deposited by the electro-spark method was 843 HV$_{0.04}$. After laser treatment, the microhardness became 784 HV$_{0.04}$, indicating laser treatment reduced the coating hardness [20].

Figure 7. SEM of HA coatings sprayed at different arc currents: (**a**) 250 A; (**b**) 450 A; and (**c**) 500 A [27].
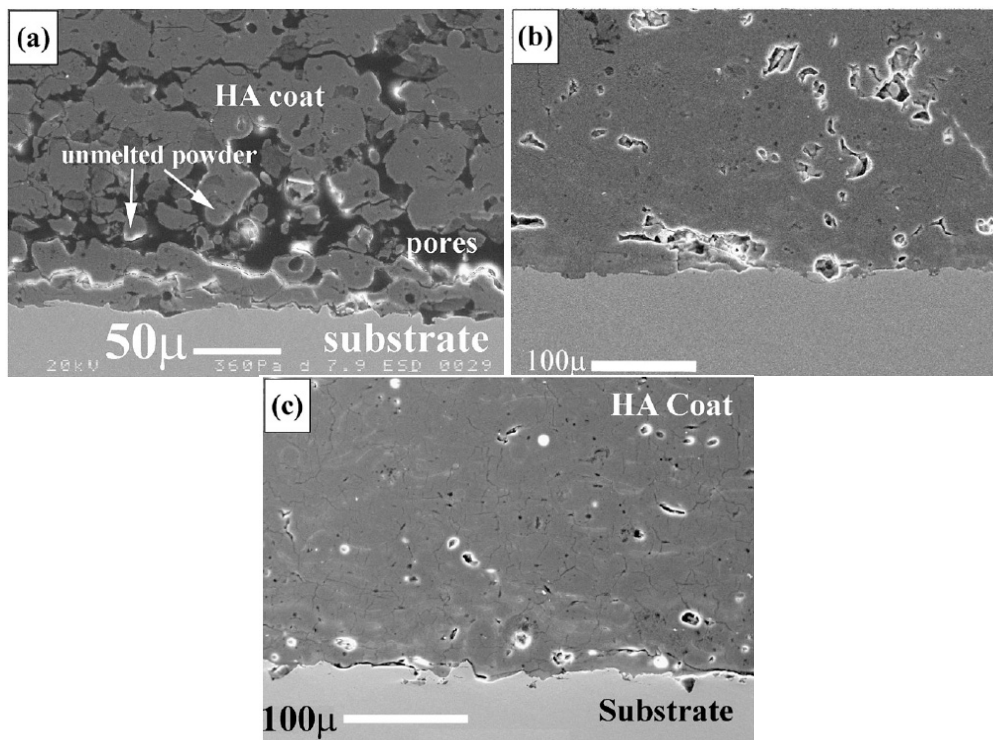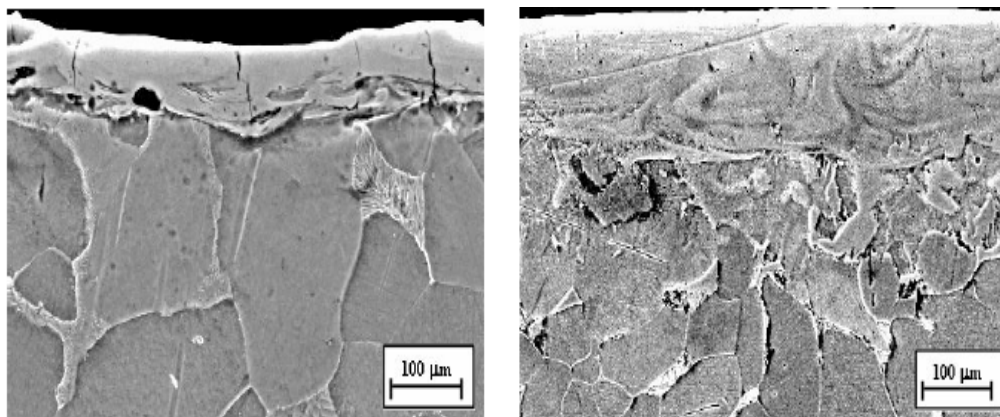

Figure 8. Microstructure in the electrospark alloying WC-Co-Al$_2$O$_3$ coating before and after treatment with Nd:YAG laser [20].

As one of the most widely used materials, steel usually is strengthened by using the nitrocarburizing method. When DC53 tool steel was nitrocarburized at 570 °C for several hours, the compound layers were composed mainly of ε-nitride (Fe$_3$N) and a small amount of γ-nitride (Fe$_4$N). The nitrocarburizing treatment not only increased the hardness but also decreased the friction coefficient of the specimen. The anti-abrasive property of the nitrocarburized specimen was found to be related to the increase in the depth of the diffusion zone. After nitrocarburizing, the severe adhesive wear was replaced by a relatively milder abrasive wear [18]. The microhardness of nitrocarburized DC53 tool steel increased with increasing treatment holding time. The 6-h nitrocarbuized specimen had the highest value (1120 HV$_{0.05}$), while the 2-h one had the lowest (980 HV$_{0.05}$) [18].

Toughness of the coatings are illustrated using Figure 9. According to Hooke's law $\sigma = E\varepsilon$, where σ is the stress, ε is the strain, if formation of a material with a higher elastic deformation is needed, its Young's modulus E must be reduced. The stress σ *versus* strain ε dependences for brittle, tough and resilient hard coatings are schematically displayed in Figure 9. Superhard materials are very brittle, exhibiting almost no plastic deformation and very low strain ($\varepsilon = \varepsilon_1$) to a rupture. Hard and tough materials exhibit both elastic and plastic deformations. The material withstanding a higher strain ($\varepsilon_1 << \varepsilon \leq \varepsilon_{max}$) without cracking exhibits a higher toughness. The hardness of tough materials is higher in the case when ε_{max} is achieved at higher values of σ_{max} [28].

Figure 9. Schematic illustration of stress σ *versus* strain ε curves of superhard (brittle), hard (tough) and hard (resilient) coatings. Resilient coatings exhibit no plastic deformation (line 0 A) [28].
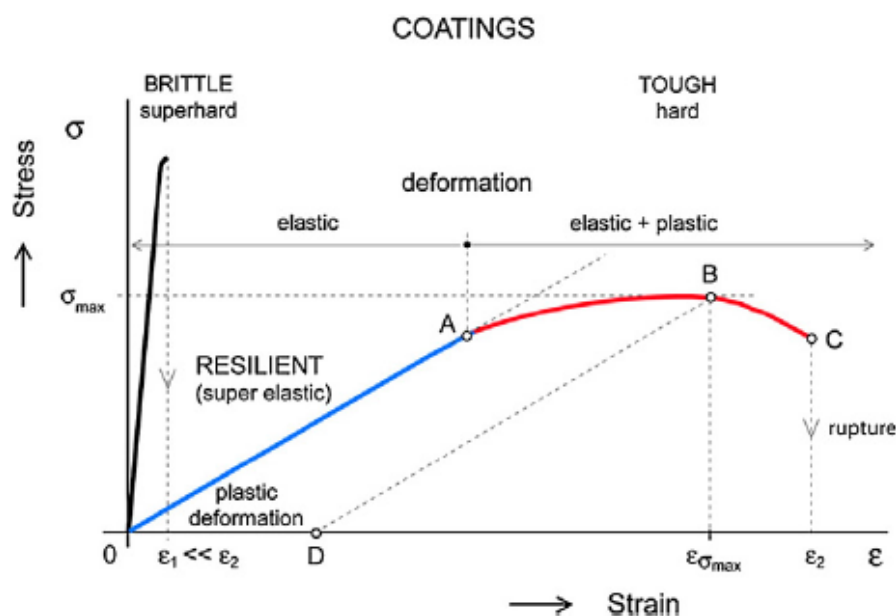
4. Multilayer and Composite Coatings

Multilayer coatings are widely used as an effective means to improve the fracture toughness of coatings, while maintaining hardness, wear resistance and other mechanical properties. In multilayer structures, the mechanisms of toughening include (see Figure 10): Crack splitting at the boundaries of small sized grains; crack deflection at the interface between layers, reduction of stress concentration by interface opening; and plastic deformation at the interface for energy dissipation and stress relaxation, "nanoplasticity" [29].

TiAlSiN/CrAlYN films synthesized on cemented carbide, silicon and SUS304 substrates with a period of 8.7 nm exhibited the highest hardness with 37.1 GPa, which was higher than the value of TiAlSiN monolayer and CrAlYN monolayer (Figure 11) [30].

Figure 10. Mechanisms of toughness enhancement in hard ceramic multilayers [29].
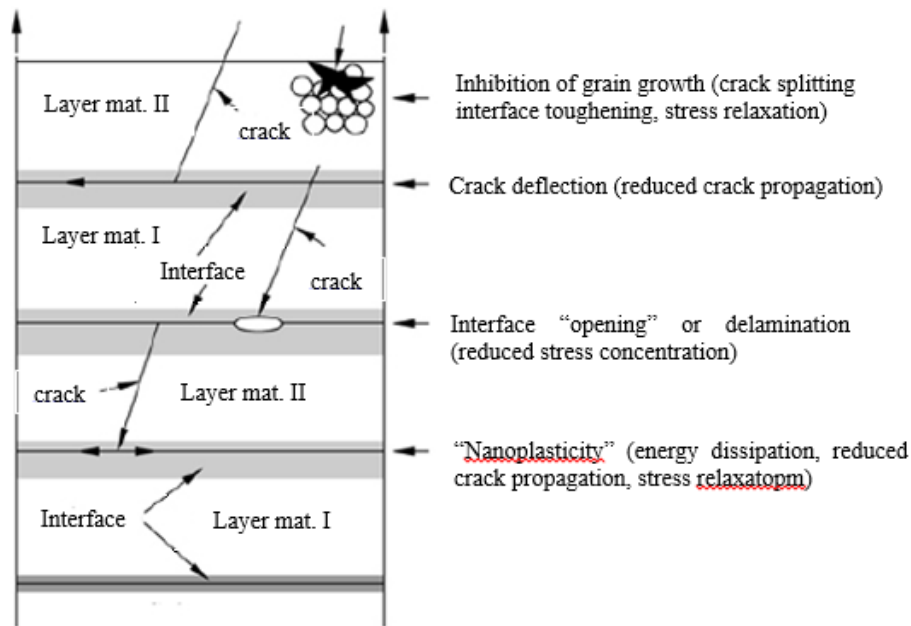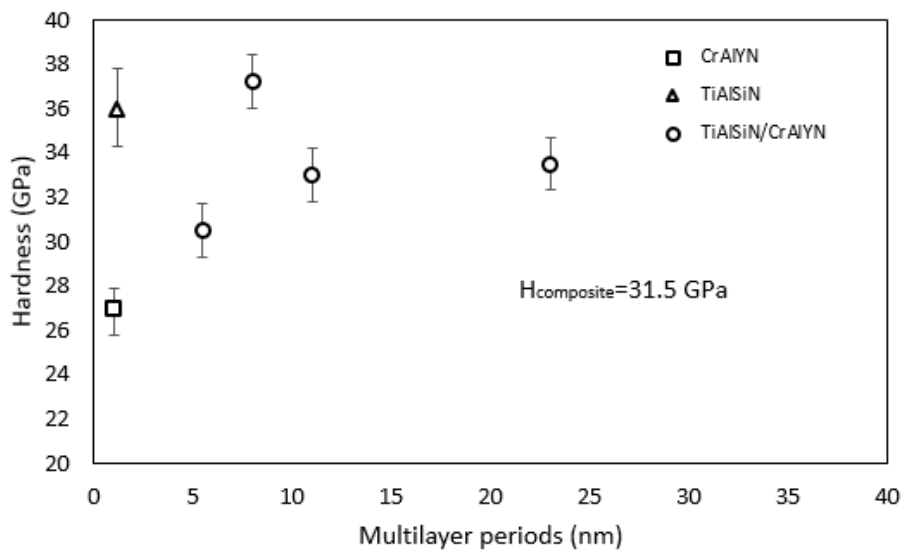

Figure 11. Vickers microhardness of the multilayer films as a function of the multilayer period [30].


Zhang *et al.* found the multilayer diamond-like carbon (DLC) films deposited at a bias alternating between −120 and −160 V almost doubled the toughness of monolayer DLC films and had better wear behaviors (Figure 12). The multilayer structure with a low modulus ratio contributed to reduced stress concentration in harder sub-layer, thereby inhibiting crack initiation [31].

Figure 12. Wear rate of monolayer DLC films and multilayer DLC films as a function of substrate bias [31].
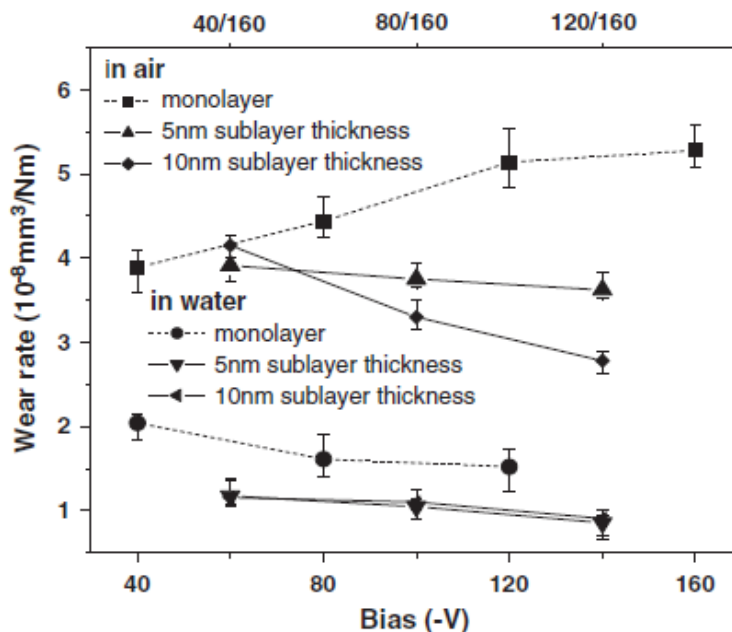
Nanocomposite coatings provide similar advantages as multilayers, while without limitations of thickness and substrate geometry. The main mechanisms responsible for increased hardness and toughness are [28] (Figure 13): Dislocation-induced plastic deformation; nanostructure of materials; and cohesive forces between atoms. The dislocation-induced plastic deformation dominates in the materials composed of large grains with sizes >10 nm. On the contrary, the nanostructure is dominant in materials composed of small grains with sizes ≤10 nm.

Figure 13. Schematic illustration of coating hardness as a function of the size d of grains [28].
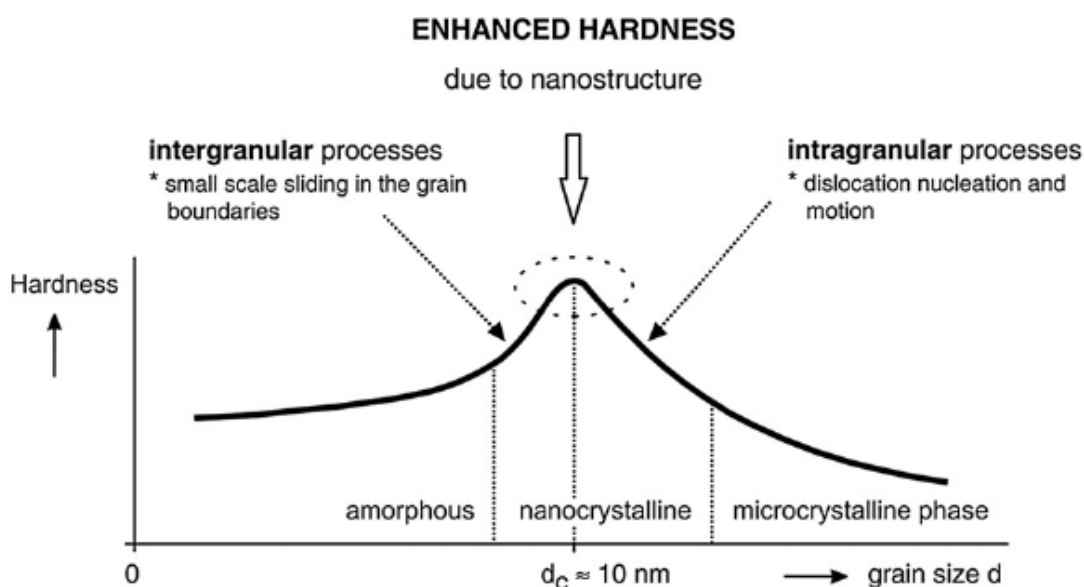
When grain sizes in such composites are reduced to a nanometer level, dislocation activity as a source of ductility is eliminated. However, these types of composites contain a high volume of grain

boundaries with a crystalline/amorphous transition across grain-matrix interfaces, limiting initial crack sizes and helping to deflect and terminate growing cracks. These mechanisms may explain the brittle resistance of novel superhard composites [32]. Li *et al.* reported the incorporation of alumina nanoparticles can increase the micro-hardness and wear resistance of electroless $Ni-P/Al_2O_3$ nanocomposite coatings (Figure 14) [33].

Figure 14. The friction coefficient of electroless Ni-P coatings (heat-treated at 300 °C for 90 min) at various particle concentrations under dry sliding conditions [33].
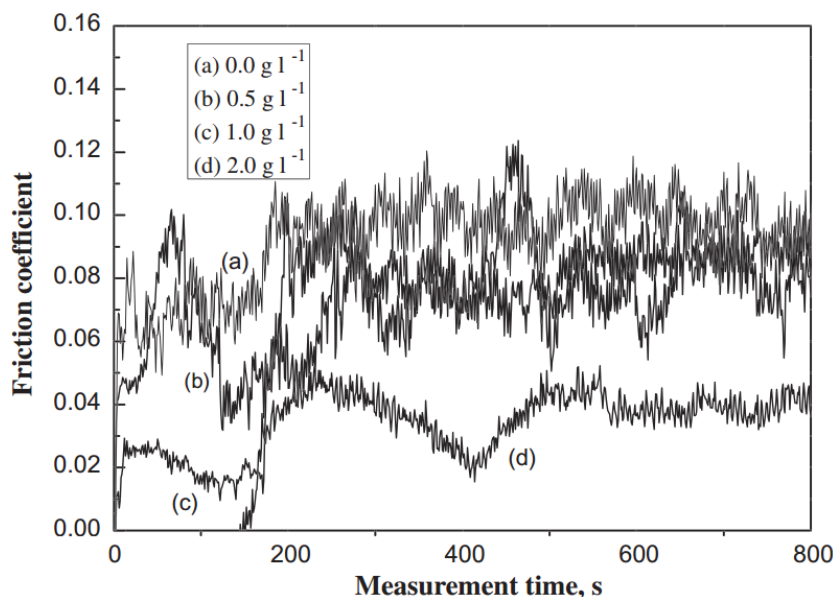

Bakhit *et al.* found the maximum microhardness of 651 HV was obtained for the Ni-Co/SiC nanocomposite coatings deposited at the optimum conditions corresponding to the maximum incorporation of the SiC nano-particles of 20 v%. The strengthening mechanism induced by the SiC nano-particles was found to be the hindering of the grain boundary mediated processes [34].

Ali reported the average microhardness value of ceramic nanocomposite coatings fabricated from lithium sulphated zirconium silicate bath was approximately 8.5 times higher than that of the as-received aluminum [35].

Combination of the nanocrystalline/amorphous designs with a functionally graded interface provides high cohesive toughness and high interface toughness in a single coating. The large fraction of grain boundary phase provides ductility through activating grain boundary slip and crack termination by nanocrack splitting. This provided a unique combination of high hardness and toughness in these coatings. Figure 15 shows Vickers indentations of YSZ-Au coating. There were no observable cracks in these coatings, even after significant substrate compliance [36].

Ranand *et al.* studied $Ti-TiB_2$ nanocomposite coatings using dual-cathode magnetron sputtering in Ar onto polished titanium and silicon substrates. $Ti-TiB_2$ nanocomposite coatings exhibited a flatter hardness-toughness relationship compared with metal carbide-DLC and $TiN-Si_3N_4$ nanocomposite coatings, since the formation of coherent $Ti-TiB_2$ interfaces, which produced stress fields activating the motion of nearby dislocations within the Ti matrix and hence improved fracture toughness [37].

Figure 15. Vickers indentation sites on the surface of YSZ-Au films with varying gold content: (**a**) 5; (**b**) 12; and (**c**) 35 at % Au [36].
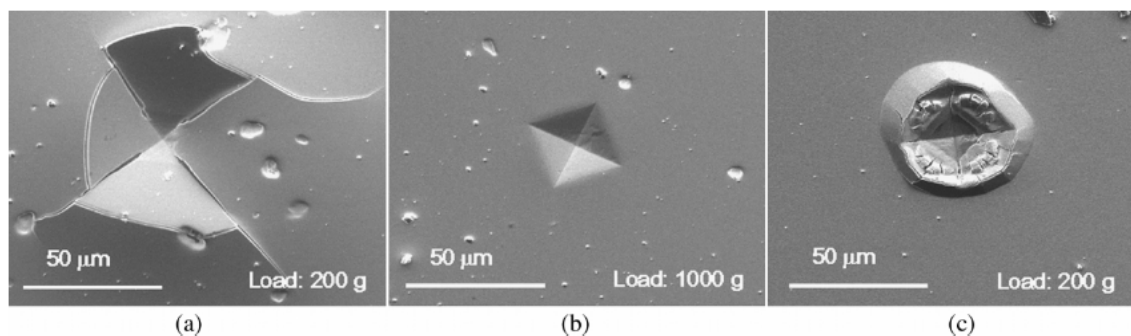
Movahedi reported the NiAl-15 wt% (Al_2O_3-13% TiO_2) nanocomposite coating was tougher and harder than the NiAl intermetallic coating. The wear behavior is attributed to the high fracture toughness of the nanocomposite coating rather than to the brittle NiAl intermetallic coating. The average specific wear rate for NiAl-15 wt% (Al_2O_3-13% TiO_2) nanocomposite coating was measured to be $0.78 \pm 0.33 \times 10$–15 m^3/N·m, much less than that for NiAl intermetallic coating. SEM micrographs of the wear track are shown in Figure 16. The changes in the wear resistance between NiAl intermetallic and NiAl-15 wt% (Al_2O_3-13% TiO_2) nanocomposite coatings were attributed to the changes in the susceptibility to crack propagation by adding Al_2O_3-13% TiO_2 nanoparticles as the reinforcing materials [38].

Figure 16. (**a**) SEM micrographs of the wear track; (**b**) Surface profile of worn surface; and (**c**) Wear debris of the NiAl-15 wt% (Al_2O_3-13% TiO_2) nanocomposite HVOF coating [38].
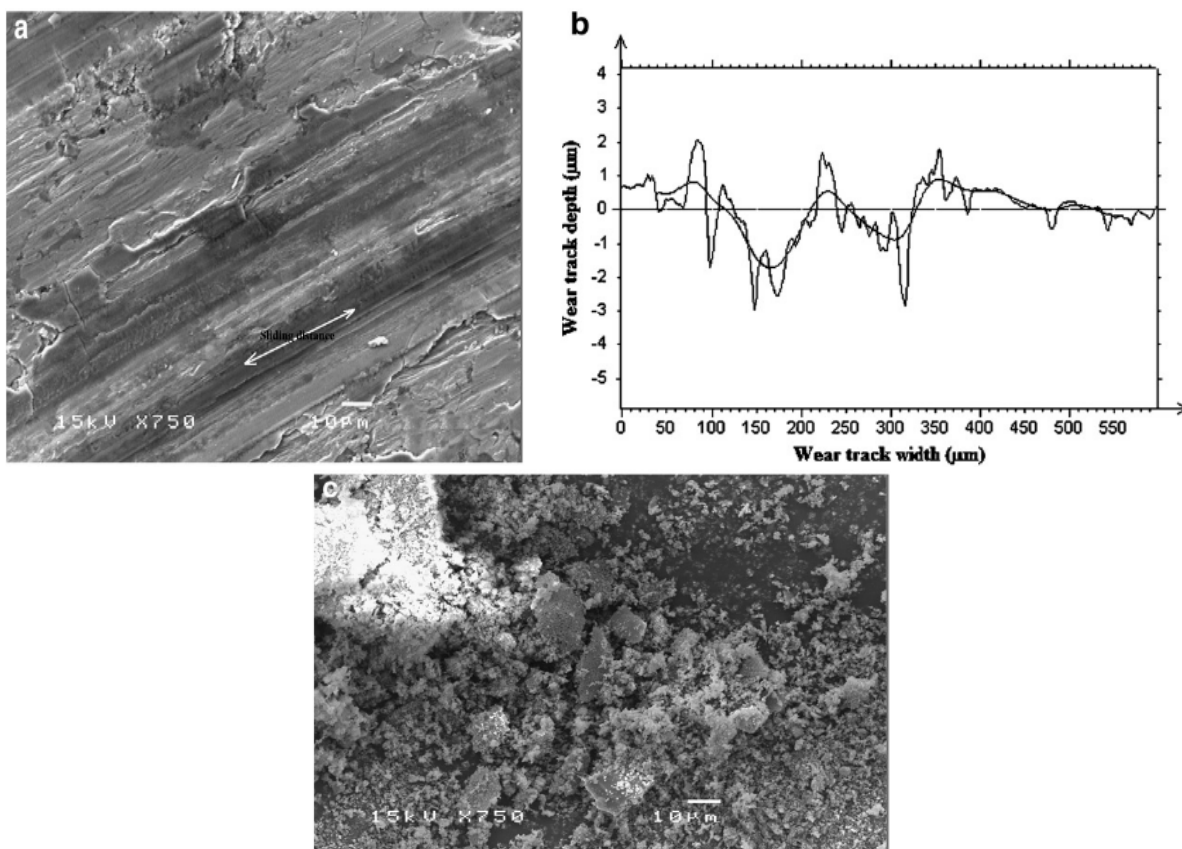
To reduce the friction coefficients and improve the anti-abrasive properties, Ni-based alloy coatings reinforced by TiC particles, graphite/TiC/Ti based alloys (GTN) were prepared on the surface of carbon steel [39]. The addition of graphite to the GTN coatings can greatly reduce the friction coefficients and enhance the wear resistance. Under a low load, the wear mechanisms of the GTN coating were mainly multi-plastic deformation with slightly abrasive wear and gradually changed into a mixture of multi-plastic deformation, delamination, and micro-cutting wear with the increase of graphite fraction. As the load increased, the main wear mechanism gradually changed from micro-cracks, micro-cutting, and adhesive wear to micro-cutting and micro-fracture with the increase of graphite fraction [39].

Nickel composites with various ceramic particles, such as Al_2O_3, SiC, B_4C, SiO_2, WC, and TiC, prepared by the composite plating method using an ethanol based nickel bath can produce better anti-abrasive coatings. Particles can be easily co-deposited with nickel in the ethanol bath. But most hydrophilic particles like SiO_2 can be hardly co-deposited from a non-aqueous metal plating bath. From wear experiments of these coatings, it can be concluded that the anti-abrasive property of a nickel-ceramic coating from the ethanol bath is much better than that of the same nickel-ceramic from the water plating bath [40].

Electroless nickel (EN) plating is an auto-catalytic reaction used to deposit a coating of nickel on a substrate. Unlike electroplating, it is not necessary to pass an electric current through the solution to form a deposit. This plating technique is to prevent corrosion and wear. EN techniques can also be used to manufacture composite coatings by suspending powder in the bath [41]. Electroless nickel plating has several advantages *versus* electroplating. Free from flux-density and power supply issues, it provides an even deposit regardless of workpiece geometry, and with the proper pre-plate catalyst, can deposit on non-conductive surfaces [42].

Vitry *et al.* [43] investigated the mechanical and wear properties of electroless nickel-boron coatings. The hardness of the deposits increased from 900 to 1250 $HV_{2.5}$ due to optimal crystallization of the nanocrystalline coating after heat treatment at 400 °C for 1 h. This increase of hardness is due to both the Hall-Petch effect and to phase transformation that occurs during heat treatment from supersaturated nickel to nickel boride. The heat treated coatings showed a good response to the wear test, without spalling nor delamination (Figure 17), with an overall metallic ductile behavior throughout the tests [43].

The tribological performance of electroless nickel or bronze can be further improved with the introduction of polytetrafluoroethylene (PTFE) particles (Figures 18 and 19) [44]. The coating covered workpiece surfaces very well without any defects even at the corners, which enhanced the break-in period for highly polished, critical surfaces of the molding cavity or core.

Figure 17. Observation of the scratch tracks up to 150 N on a 25 μm thick electroless nickel-boron coating after heat treatment at 400 °C for 1 h [43].
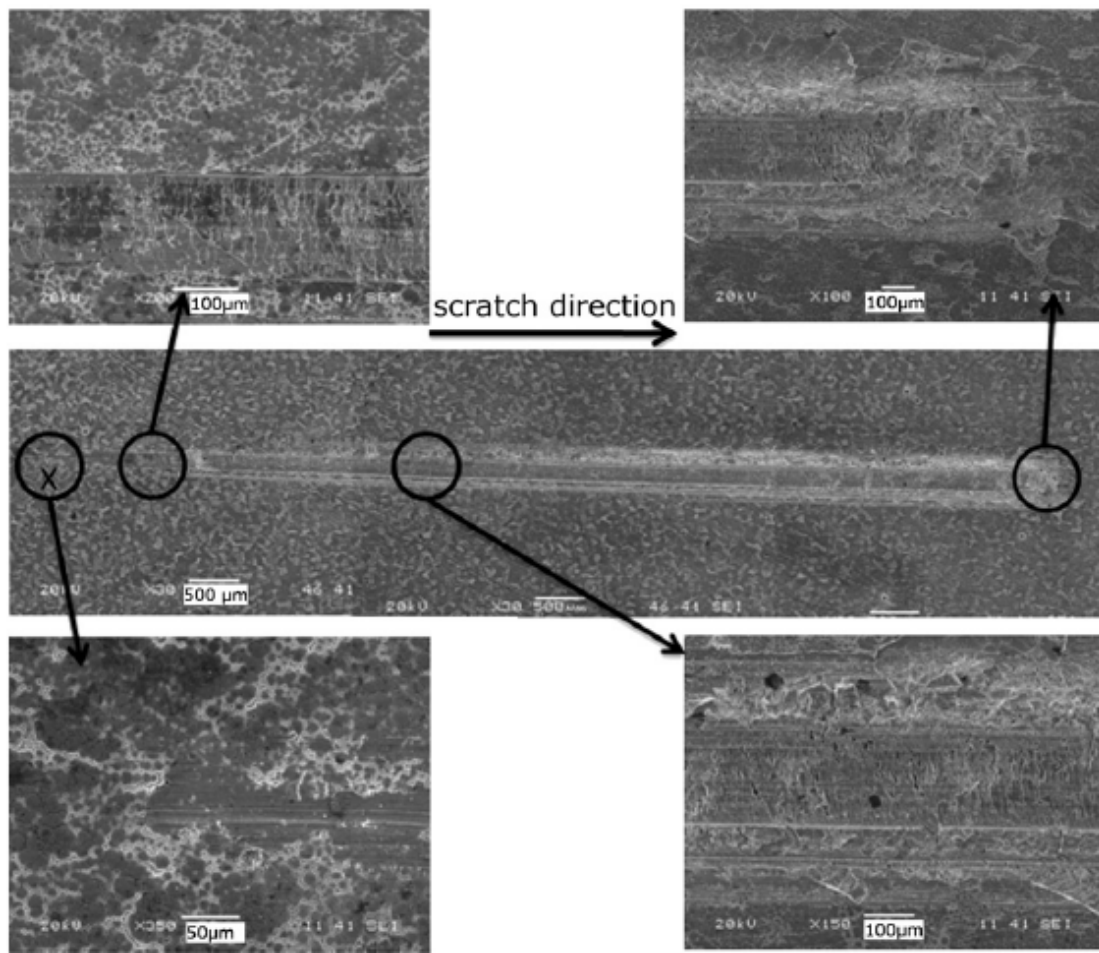

Figure 18. Scanning electron micrograph of the surface of nickel with PTFE protected sample [44].
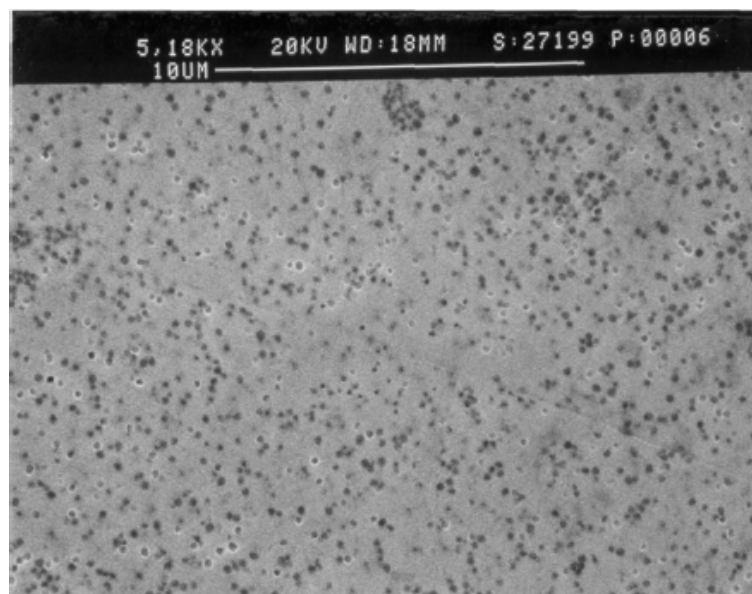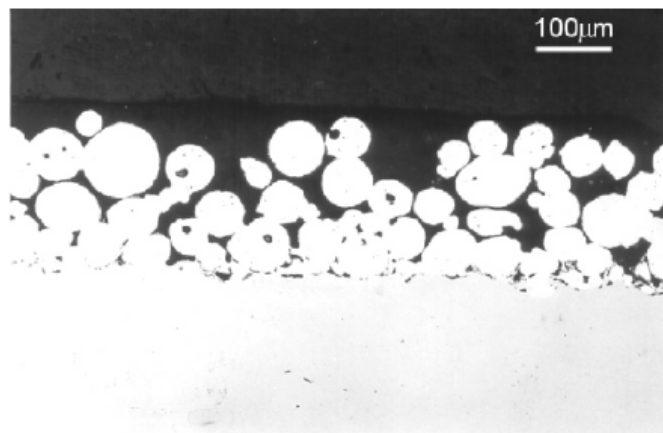
Figure 19. Optical micrograph of the cross section of the sample protected with bronze particles in a PTFE matrix [44].

5. Ceramic Anti-Abrasive Coating

Ceramic coating can be used on the surface of metal or ceramic materials. Since ceramic has relatively high hardness, corrosion resistance and heat resistance, it can be widely used as a protection coating. Typical ceramic coatings include Al_2O_3/TiO_2, $SiO_2/TiO_2/Cr_2O_3$, SiC, B_4C, ZrO_2, CaO, CrN/AlCrN, CrN/BCN, SiO_2, WC, and TiC.

It was found that the property and microstructure of the coatings are affected by the critical spray process parameters (CPSP). The specific parameter of the spray condition is determined by optimization of the coating spray process and the anti-abrasive performance. The coating powder can be reconstructed into plasma sprayable size agglomerates by controlling CPSP and adding additives. The reconstruction process of plasma sprayed coating included an additional step of plasma processing, during which the reconstructed spraying powders were pre-heated and air-quenched in a collection chamber. Figure 20 shows the cross-section view of different sprayed powders. Nanostructured Al_2O_3 and 13 wt% TiO_2 coating powders were mixed and reconstituted to a size that is suitable to spray. The α-Al_2O_3 were shown in black. The TiO_2 grains were dissolved in oxide additives for the modified powders, and are shown in bright regions [45].

From Figure 21, it can be found that the reconstituted coating has a significant improvement in the anti-abrasive performance. Through a broad range of mechanical properties testing of the nanostructured alumina-titanium oxidize coating, it was found that the nanostructured coating exhibited a superior anti-abrasive performance [45]. AlCrN (high aluminum-content) coating can be deposited by the multi-arc plating technique. Since the physical vapor deposited (PVD) CrN coating has a relatively good oxidation, anti-corrosive, and anti-adhesive properties, it can be widely used in industrial applications. It has been found that CrN and aluminum alloy composite shows a significant increase in hardness and has remarkable anti-abrasive performance. From the reciprocating sliding tribological behavior testing of the AlCrN coating against Si_3N_4 ceramic and pure titanium balls, it can be illustrated that the AlCrN coating showed a significant improvement in wear debris removal efficiency and load-carrying capacity as compared to the CrN coating. The CrN coating suffered severe concentrated wear under high normal load conditions [22].

Figure 20. Backscattered electron micrographs of (**a**) Metco-130 powders and reconstituted (**b**) Al$_2$O$_3$-13 wt% TiO$_2$ without the additives and (**c**) Al$_2$O$_3$-13 wt% TiO$_2$ with the additives [45].
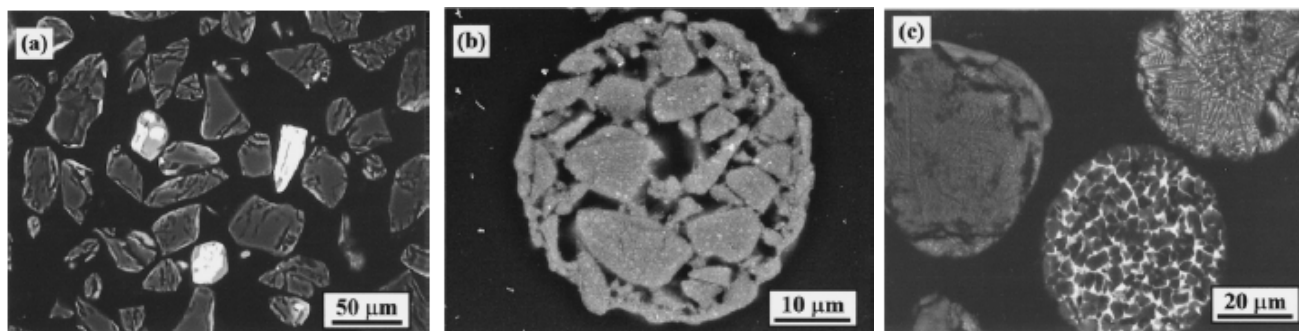
Figure 21. Surface morphology of sprayed coating (**a**,**c**) Metco-130 (**b**,**d**) reconstituted nanostructured Al$_2$O$_3$-13 wt% TiO$_2$ coatings after the (**a**,**b**) abrasive wear and (**c**,**d**) scratch test [45].
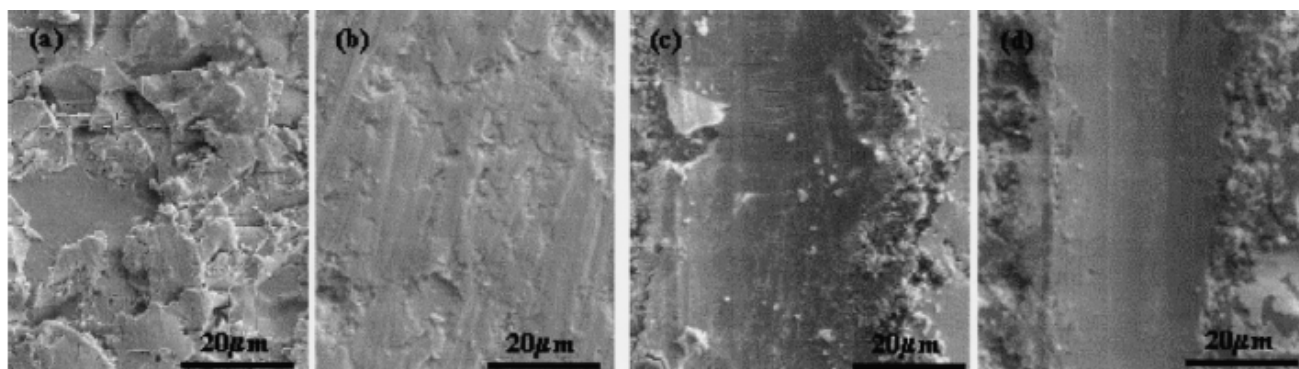
6. Polymer Coatings

Polymer can be used as typical anti-friction coating by fluidization on the metallic matrix [1]. Polymers such as PA (polyamide) or PE (polyethylene) can be directly deposited on the surface of metal materials by fluidization, where a fluid (liquid or gas) is passed up through the granular material and convert granular material from a static solid-like state to a dynamic fluid-like state. The optimal thickness of the polymer coating is about 0.3 mm. The polymer coating can reduce the friction coefficient. The utility of the thin polymeric coating instead of a thick polymeric solid element can transport heat from the wearing area faster than the thick polymer coating. When a PA coating rubs against steel, the friction coefficient was lower (below 0.15) than the thick PA elements [1].

Polymer can also be used as additives to the alloy coating and ceramic coating. When the polymer is used as the addictive, the polymer can bond the alloy grain or ceramic granular by its long molecular chains. That can link the granular extremely compact so that the composite can form a dense coating layer, thus, resisting wear. Zhu and Wang have prepared an oxide coating with additive of ethylene glycol gligmers on the AZ31B Mg alloy in an environment friendly electrolyte with additives by plasma electrolytic anodization [46]. The performance of the anodized film was investigated. The films were found mainly consisting of MgO, MgSiO$_3$, Mg$_2$SiO$_4$. The surface morphologies were more and more compact and homogenous with the increase of the PEG (polyethylene glycol). The improvement in

abrasive resistance of the anodic film formed in the electrolyte may be attributed to its much more compact surface and the incorporation of ductile PEG chains among those oxides [46].

Brzezinski *et al.* produced a thin-coat on the textile using sol-gel method. The coating can gain a great abrasive resistance performance [47]. SiO_2 and Al_2O_3 were used as the sol, and glycidoxy-propyltrimethoxy silane aluminum isopropoxide was used as precursors on the fiber/fabric surface. Comparing with the texture without any coating, the abrasion resistance of the coating has been increased by about five times [47].

7. Diamond-Like Carbon Coatings

Diamond-like carbon (DLC) exists in amorphous carbon materials that show some typical properties of diamond. Depending on the ratio of sp^2 and sp^3 bonds and hydrogen content, DLC are divided into several groups, as shown in Figure 22. The amorphous carbon (a-C) coatings with mainly sp^2 bonds are in the lower left corner of diagram. The hydrogenated amorphous carbon (a-C:H) has some hydrogen content and relatively low sp^3 bonds. Hydrocarbon polymers are located in the right corner. The sputtered hydrogenated amorphous carbon (a-C:H) has both sp^2 bonds and sp^3 bonds, and it is in the middle of the diagram. Coatings using plasma enhanced vapor deposition with more sp^3 bonds the hydrogenated tetrahedral amorphous carbon (ta-C:H). The tetrahedral amorphous carbon (ta-C) has a majority of sp^3 bonds and barely no hydrogen content [48].

Figure 22. Ternary phase diagram of sp^2, sp^3, and hydrogen contents of various forms of DLC [48].
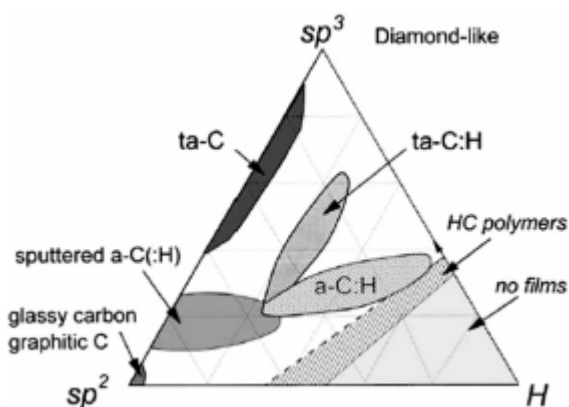
DLC coatings exhibit a combination of a low coefficient of friction and high micro-hardness, making them extremely effective in many tribological and wear applications. He *et al.* applied DLC coatings to the surface of steel bearings to reduce the negative effect of contaminants in lubricant [49]. The study showed that DLC coatings produced a very low friction and a high sliding wear resistance to improve the tribological properties and durability of running components. However, the protective coatings caused even more damage to the running components once they have been broken up by hard contaminants [49]. Corbella and Rubio-Roy prepared DLC films by plasma-enhanced chemical vapor deposition [25]. They measured the abrasive wear rate and the coefficient of friction of the DLC films deposited at different pulse frequencies and peak voltages. The surface roughness of DLC was much

higher with an increase of one order of magnitude at high peak voltage at 100 kHz, while the coefficient of friction was lowered by increasing the peak voltage [25].

Yuan and Brown's research studied the atomic structures of DLC by using electron energy loss spectroscopy (EELS) [50]. The study showed that the DLC films by using ion beam deposition consisted mostly of sp^3-bond atoms which play critical role in its mechanical rigidity and chemical inertness, but also high friction. The small amount of sp^2 carbon clusters were responsible for optical absorption gap and electric conduction [50]. The sp^2 bonding provides low friction, but also low hardness. There is, thus, a balance between achieving both high hardness and low friction.

The application problem of hydrogenated carbon coatings is their very low fracture toughness. One method to resolve this problem is to incorporate ceramic materials into a-C:H coatings. This design allows users to have moderate hardness, stiffness, good fracture resistance, and retain their good tribological properties. Cr_2C nanoparticles can be considered as energy barriers that increase fracture toughness from K_{IC} (changes of fracture toughness) = 1.55 $MPa \cdot m^{0.5}$ for the a-C:H coating up to K_{IC} = 1.7–3.4 $MPa \cdot m^{0.5}$ for nanocomposite coatings. And the lowest wear index found for Cr_2C/a-C:H coatings was about seven times smaller than for a-C:H coatings [51].

Working conditions or contact parameters are one important factor in DLC coating performance. Bremond *et al.* [52] found friction increase tremendously at high temperature due to the ruin of DLC coatings (see Figure 23). High friction is related with the presence of titanium and metallic particles in the contact [52].

Figure 23. Influence of working temperature on coefficient of friction of a-C:H coating [52].
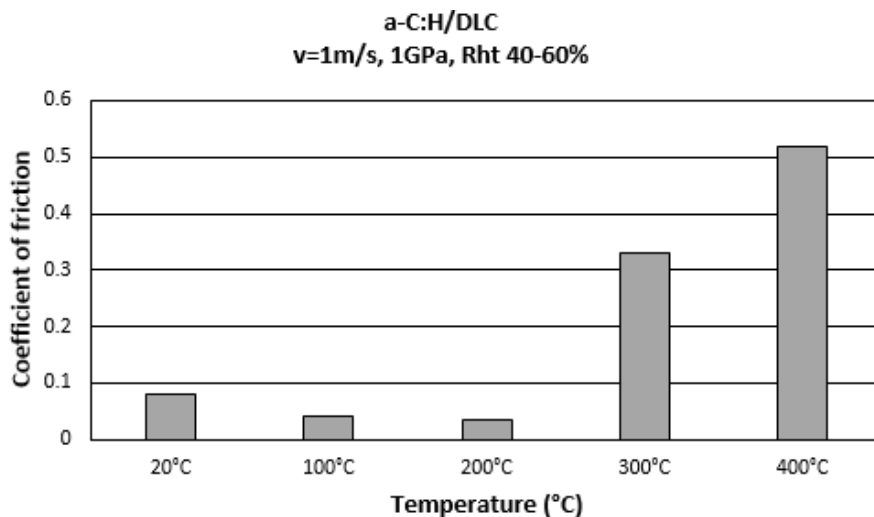
The hydrogen content in DLC coatings can significantly affect the tribology properties of these coatings. DLC coatings with hydrogen content have low coefficient of friction about 0.05 in dry air. The elimination of strong covalent bond and better shielding of carbon atoms by dehydration lead to this phenomenon [53]. It is well known that chemically active gas can have strong effect on the frictional properties of DLC coatings. Erdemir [53] found DLC coating performance is humidity dependent. As long as the test environment is inert and dry, the friction coefficients of hydrogen-free are general be high, whereas those of the hydrogen-rich films would be low. As shown in Figure 24, after humidity

added, the friction coefficient dropped to 0.25, whereas the friction coefficient of hydrogenated films increased to 0.06 [53].

The doping of DLC coating with different metals can change mechanical properties and tribological properties of coatings. Wei *et al.* investigated the mechanical properties of diamond-like carbon (DLC) thin films that contain foreign atoms, prepared by pulsed laser deposition [54]. Wear tests show improved wear resistance in the copper doped DLC coatings. Nanoindentation results give an average hardness above 40 GPa and effective Young's modulus above 200 GPa for pure DLC. The copper doped DLC films showed slightly decreased hardness and Young's modulus as compared to pure DLC films. Ti-DLC films with low concentration Ti doping exhibit low wear rate of $2.0 \pm 0.2 \times 10^{-8}$ mm^3/Nm and a low friction coefficient of about 0.04 [55].

Figure 24. Effect of humidity on friction coefficient of hydrogen-free and hydrogenated DLC films [52].
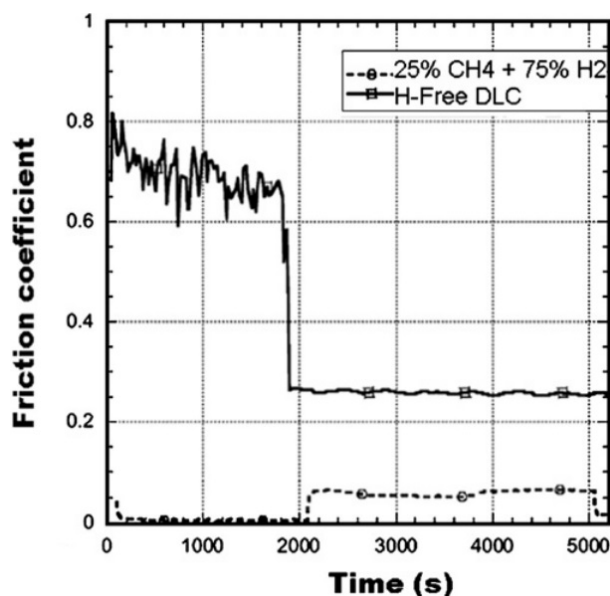
8. Conclusions

This article reviews all major types of abrasive resistant coatings, including metal, ceramic, polymer coatings, and diamond-like carbon coatings. Multilayer and composite coatings are discussed. The relevant properties and preparation methods of the various coatings are also summarized. The properties can be modified through selecting coating materials and processing methods.

Conflicts of Interest

The authors declare no conflict of interest.

References

1. Zygmunt, R. Special Tribological Coatings. In *Tribology Series*; Elsevier: Amsterdam, The Netherlands, 1989; Volume 13, pp. 269–301.
2. Rabinowicz, E. *Friction and Wear of Materials*; Wiley: New York, NY, USA, 1965.

3. Bhushan, B. *Introduction to Tribology*; Wiley: New York, NY, USA, 2002.

4. Rabinowicz, E. *Friction and Wear of Materials*, 2nd ed.; Wiley: New York, NY, USA, 1995.

5. Khruschov, M.M. Principles of abrasive wear. *Wear* **1974**, *28*, 69–88.

6. ASTM. *Standard Terminology Relating to Wear and Erosion*; ASTM: West Conshohocken, PA, USA, 1987.

7. ASM. Friction, Lubrication, and Wear Technology. In *ASM Handbook*; ASM International: Materials Park, OK, USA, 1992.

8. Barwell, F.T. *Plugging the Tribological Leak*; Production Engineering Research Association: Bingley, UK, 1969.

9. Williams, J.A.; Hyncica, A.M. Mechanisms of abrasive wear in lubricated contacts. *Wear* **1992**, *152*, 57–74.

10. Goddard, H.W.J. A theory of friction and wear during the abrasion of metals. *Wear* **1962**, *5*, 114–135.

11. Da Silva, W.M.C.; de Mello, H.L. Transitions in abrasive wear mechanisms: Effect of the superimposition of interactions. *Wear* **2011**, *271*, 977–986.

12. Buijs, M.; Houten, K.K. Three-body abrasion of brittle materials as studied by lapping. *Wear* **1993**, *166*, 237–245.

13. Pellegrin, D.V.D.; Torrance, A.A. Characterisation of abrasive particles and surfaces in grinding. Available online: http://hdl.handle.net/2262/10918 (accessed on 5 April 2013).

14. Gahr, K.H.Z. *Microstrucutre and Wear of Materials*; Elsevier: New York, NY, USA, 1987.

15. Fallqvist, M. Microstructural, Mechanical and Tribological Characterisation of CVD and PVD Coatings for Metal Cutting Applications. Doctoral Thesis, Uppsala University, Acta Universitatis Upsaliensis, Uppsala, Sweden, 2012.

16. Ludema, K. Friction, Wear, Lubrication: A Textbook in Tribology; CRC Press: Boca Raton, FL, USA, 1996.

17. De Garmo, E.P.; Black, J.T.; Kohser, R.A. *DeGarmo's Materials and Processes in Manufacturing*; Wiley: New Jersey, NJ, USA, 2011.

18. Wen, D.-C. Erosion and wear behavior of nitrocarburized DC53 tool steel. *Wear* **2010**, *268*, 629–636.

19. Ma, C.; Zhang, M.; Yuan, Y.; Jing, X.; Bai, X. Tribological behavior of plasma electrolytic oxidation coatings on the surface of Mg–8Li–1Al alloy. *Tribol. Int.* **2012**, *47*, 62–68.

20. Radek, N.; Bartkowiak, K. Performance properties of electro-spark deposited carbide-ceramic coatings modified by laser beam. *Phys. Procedia* **2010**, *5*, 417–423.

21. Mezlini, S.; Kapsa, P.; Henon, C.; Guillemenet, J. Abrasion of aluminium alloy: Effect of subsurface hardness and scratch interaction simulation. *Wear* **2004**, *257*, 892–900.

22. Mo, J.L.; Zhu, M.H. Sliding tribological behaviors of PVD CrN and AlCrN coatings against Si_3N_4 ceramic and pure titanium. *Wear* **2009**, *267*, 874–881.

23. Zhang, J.; Tian, B.; Wang, C. Long-term surface restoration effect introduced by advanced silicate based lubricant additive. *Tribol. Int.* **2013**, *57*, 31–37.

24. Aihua, L.; Jianxin, D.; Haibing, C.; Yangyang, C.; Jun, Z. Friction and wear properties of TiN, TiAlN, AlTiN and CrAlN PVD nitride coatings. *Int. J. Refract. Met. Hard Mater.* **2012**, *31*, 82–88.

25. Corbella, C.; Rubio-Roy, M.; Bertran, E.; Polo, M.C.; Pascual, E.; Andújar, J.L. Low friction and protective diamond-like carbon coatings deposited by asymmetric bipolar pulsed plasma. *Diam. Relat. Mater.* **2009**, *18*, 1035–1038.

26. Meyers, M.A.; Chawla, K.K. *Mechanical Behavior of Materials*; Cambridge University Press: New York, NY, USA, 1999.

27. Morks, M.F.; Kobayashi, A.; Fahim, N.F. Abrasive wear behavior of sprayed hydroxyapitite coatings by gas tunnel type plasma spraying. *Wear* **2007**, *262*, 204–209.

28. Musil, J. Hard nanocomposite coatings: Thermal stability, oxidation resistance and toughness. *Surf. Coat. Technol.* **2012**, *207*, 50–65.

29. Voevodin, A.A.; Zabinski, J.S.; Muratore, C. Recent advances in hard, tough, and low friction nanocomposite coatings. *Tsinghua Sci. Technol.* **2005**, *10*, 665–679.

30. Mori, T.; Noborisaka, M.; Watanabe, T.; Suzuki, T. Oxidation resistance and hardness of TiAlSiN/CrAlYN multilayer films deposited by the arc ion plating method. *Surf. Coat. Technol.* **2012**, *213*, 216–220.

31. Zhang, Y.; Zhai, Y.; Li, F.; Zhang, S.; Zhang, P.; Zhang, S. Effect of microstructure and mechanical properties difference between sub-layers on the performance of alternate hard and soft diamond-like carbon multilayer films. *Surf. Coat. Technol.* **2013**, *232*, 575–581.

32. Veprek, S. The search for novel, superhard materials. *J. Vac. Sci. Technol. A* **1999**, *17*, 2401–2420.

33. Li, C.; Wang, Y.; Pan, Z. Wear resistance enhancement of electroless nanocomposite coatings via incorporation of alumina nanoparticles prepared by milling. *Mater. Des.* **2013**, *47*, 443–448.

34. Bakhit, B.; Akbari, A. Synthesis and characterization of Ni-Co/SiC nanocomposite coatings using sediment co-deposition technique. *J. Alloys Compd.* **2013**, *560*, 92–104.

35. Mubarak Ali, M.; Raj, V. Formation and characterization of ceramic nanocomposite crystalline coatings on aluminium by anodization. *J. Mater. Sci. Technol.* **2013**, *29*, 595–602.

36. Voevodin, A.A.; Hu, J.J.; Jones, J.G.; Fitz, T.A.; Zabinski, J.S. Growth and structural characterization of yttria-stabilized zirconia-gold nanocomposite films with improved toughness. *Thin Solid Films* **2001**, *401*, 187–195.

37. Ranade, A.N.; Krishna, L.R.; Li, Z.; Wang, J.; Korach, C.S.; Chung, Y.-W. Relationship between hardness and fracture toughness in Ti-TiB$_2$ nanocomposite coatings. *Surf. Coat. Technol.* **2012**, *213*, 26–32.

38. Movahedi, B. Fracture toughness and wear behavior of NiAl-based nanocomposite HVOF coatings. *Surf. Coat. Technol.* **2013**, *235*, 212–219.

39. Cai, B.; Tan, Y.-F.; Tu, Y.-Q.; Wang, X.-L.; Xu, T. Effects of graphite content on microstructure and tribological properties of graphite/TiC/Ni-base alloy composite coatings. *Trans. Nonferrous Met. Soc. China* **2011**, *21*, 1741–1749.

40. Curran, J.A.; Clyne, T.W. Thermo-physical properties of plasma electrolytic oxide coatings on aluminium. *Surf. Coat. Technol.* **2005**, *199*, 168–176.

41. Sudagar, J.; Lian, J.; Sha, W. Electroless nickel, alloy, composite and nano coatings—A critical review. *J. Alloys Compd.* **2013**, *571*, 183–204.

42. Rhodes, J.; Wachsman, E.D. Mixed Protonic Electronic Barium Cerates for Hydrogen Separation. In *Solid State Ionic Devices II—Ceramic Sensors*; The Electrochemical Soceity: New Jersey, NJ, USA, 2001; pp. 2000–2032.

43. Vitry, V.; Kanta, A.-F.; Delaunois, F. Mechanical and wear characterization of electroless nickel-boron coatings. *Surf. Coat. Technol.* **2011**, *206*, 1879–1885.

44. Rossi, S.; Chini, F.; Straffelini, G.; Bonora, P.L.; Moschini, R.; Stampali, A. Corrosion protection properties of electroless Nickel/PTFE, Phosphate/MoS$_2$ and Bronze/PTFE coatings applied to improve the wear resistance of carbon steel. *Surf. Coat. Technol.* **2003**, *173*, 235–242.

45. Czerwinski, F. Thermochemical Treatment of Metals. In *Heat Treatment—Conventional and Novel Applications*; Intech: Rijeka, Croatia, 2012.

46. Zhu, F.; Wang, J.; Li, S.; Zhang, J. Preparation and characterization of anodic films on AZ31B Mg alloy formed in the silicate electrolytes with ethylene glycol oligomers as additives. *Appl. Surf. Sci.* **2012**, *258*, 8985–8990.

47. Brzeziński, S.; Kowalczyk, D.; Borak, B.; Jasiorski, M.; Tracz, A. Applying the sol-gel method to the deposition of nanocoats on textiles to improve their abrasion resistance. *J. Appl. Polym. Sci.* **2012**, *125*, 3058–3067.

48. Sedlaček, M.; Podgornik, B.; Vižintin, J. Tribological properties of DLC coatings and comparison with test results: Development of a database. *Mater. Charact.* **2008**, *59*, 151–161.

49. He, F.; Wong, P.L.; Zhou, X. Wear properties of DLC-coated steel rollers running with highly contaminated lubrication. *Tribol. Int.* **2010**, *43*, 990–996.

50. Yuan, J.; Brown, L.M. Investigation of atomic structures of diamond-like amorphous carbon by electron energy loss spectroscopy. *Micron* **2000**, *31*, 515–525.

51. Kot, M.; Major, Ł.; Chronowska-Przywara, K.; Lackner, J.M.; Waldhauser, W.; Rakowski, W. The advantages of incorporating Cr$_x$C nanograins into an a-C:H matrix in tribological coatings. *Mater. Des.* **2014**, *56*, 981–989.

52. Bremond, F.; Fournier, P.; Platon, F. Test temperature effect on the tribological behavior of DLC-coated 100C6-steel couples in dry friction. *Wear* **2003**, *254*, 774–783.

53. Erdemir, A. The role of hydrogen in tribological properties of diamond-like carbon films. *Surf. Coat. Technol.* **2001**, *146–147*, 292–297.

54. Wei, Q.; Sharma, A.K.; Sankar, J.; Narayan, J. Mechanical properties of diamond-like carbon composite thin films prepared by pulsed laser deposition. *Compos. Part B* **1999**, *30*, 675–684.

55. Qiang, L.; Zhang, B.; Zhou, Y.; Zhang, J. Improving the internal stress and wear resistance of DLC film by low content Ti doping. *Solid State Sci.* **2013**, *20*, 17–22.